Engineering Structures 56 (2013) 1645–1657

Contents lists available at ScienceDirect

Engineering Structures

journal homepage: www.elsevier.com/locate/engstruct

Cyclic loading test for emulative precast concrete walls with partially reduced rebar section

Su-Min Kang [a,*], Ook-Jong Kim [a], Hong-Gun Park [b]

[a] Architectural Engineering and Research team, Daelim Industrial Co., 146-12, Susong-Dong, Jongno-Gu, Seoul 110-732, Republic of Korea
[b] Department of Architecture & Architectural Engineering, Seoul National University, 599 Gwanak-ro, Gwanak-gu, Seoul 151-744, Republic of Korea

ARTICLE INFO

Article history:
Received 15 June 2011
Revised 19 July 2013
Accepted 24 July 2013
Available online 29 August 2013

Keywords:
Precast concrete
Structural wall
Connection
Seismic performance
Capacity design

ABSTRACT

In conventional precast concrete (PC) walls subject to cyclic loading, the ductility and energy dissipation capacity are decreased by gap opening and shear slip at the panel joints. In this study, to enhance the earthquake resistance of emulative PC walls, two potential methods were studied. First, bonded or unbonded longitudinal rebars with partially reduced cross-sectional area were used at the plastic hinge zone. By using the reduced rebar area, the PC panel at the wall bottom was weakened to develop a plastic hinge zone in the PC panel rather than at the panel joints. Second, a RC–PC hybrid wall was considered, where cast-in-place concrete was used for the plastic hinge zone at the bottom of wall. Four specimens, including an ordinary RC wall, were tested under cyclic loading. The test results revealed that gap opening and shear slip at the panel joints were prevented by using the proposed methods. As a result, the ductility and energy dissipation of the proposed PC walls were comparable to those of the RC wall.

1. Introduction

In past earthquake events and experimental studies, significant damages and brittle failures were reported in emulative precast concrete (PC) walls [1–3]. The majority of the damages occurred at the panel joints which were vulnerable to shear slip and gap opening. Thus, to secure the integrity of the PC panels, special details need to be considered.

In the case of non-emulative PC walls, unbonded prestressed PC methods were developed to enhance the earthquake resistance [4–19]. By using unbonded prestressing tendons, gap opening and shear slip at the panel joints can be minimized. Further, the elastic restoring force of the unbonded tendon prevents residual lateral deformations in the PC wall (i.e. self-centering behavior [20–25]), which is advantageous in seismic retrofit after earthquake event. A disadvantage of this system is the decrease in energy dissipation capacity caused by using unbonded prestressing tendons. To enhance energy dissipation, mild steel bars can be used as a hysteretic energy dissipation device [11,13,17]. However, according to the studies conducted by Holden et al. [11] and Smith and Kurama [17], the enhancement of energy dissipation is limited, and a high initial construction cost is required.

In the case of emulative PC walls, the majority of existing studies focused on strengthening the panel joints to prevent gap opening and shear slip. Soudki et al. [26,27] studied various rebar connection methods at the PC panel joints: bonded or unbonded rebars with sleeve connections, rebars with sleeve connections and multiple shear keys, rebars welded to steel angles, and rebars bolted to steel tubes. Although the unbonded rebars with sleeve connections showed the best performance, local failures at the panel joints were not completely prevented. Han [28] tested PC walls with two different types of panel connections: rebars bolted to high-strength steel tubes and dowel bars with sleeve connections. The performance of the PC walls was directly compared with that of RC walls. Similar to the test results obtained by Soudki et al. [26,27], the PC walls exhibited insufficient stiffness, strength, deformation, and energy dissipation capacity when compared to the RC wall. In particular, the energy dissipation capacity of the PC wall was only 25% that of the RC wall, which indicates that the majority of the wall deformation was caused by the gap opening at the panel joints. The results of the existing studies reveal that it is extremely difficult to avoid gap opening at the panel joints by strengthening the panel joints. This is partly because, under cyclic loading, the connection devices used at the panel joints were not adequately anchored to the PC panels, or because the anchorage of the connection devices and the rebar splices strengthened the PC panel itself as well as the panel joint. Thus, despite the strengthening strategy for the panel joints, inelastic deformation was concentrated at the panel joints, which induced unstable behavior and low energy dissipation. Currently, American Concrete Institute (ACI) 318 [29] code requires that the earthquake resistance of emulative PC walls be equivalent to that of comparable

* Corresponding author. Tel.: +82 2 369 4569; fax: +82 2 369 4100.
E-mail addresses: ksm0626@paran.com (S.-M. Kang), kimoj@daelim.co.kr (O.-J. Kim), parkhg@snu.ac.kr (H.-G. Park).

0141-0296/$ - see front matter © 2013 Elsevier Ltd. All rights reserved.
http://dx.doi.org/10.1016/j.engstruct.2013.07.036

Nomenclature

A	gross cross-sectional area
c	depth of compression zone at the maximum moment
c_y	depth of compression zone at the yield moment
f'_c	compressive strength of concrete
f_y	steel yield stress
h	height from the base to the loading point
h'	height from the flexural critical section to the loading point
l	wall depth
M	bending moment
P	axial load
V	lateral load
V_{max}	maximum lateral load
$V_{pre.}$	predicted maximum lateral load
$V_{pre.(s)}$	predicted shear strength at PC panel joints
V_u	post-peak load corresponding to 90% of V_{max}
V_y	yield load
ε_y	yielding strain of vertical rebar
ε_{cmax}	ultimate compressive strain of concrete
Δ_o	displacement at maximum load V_{max}
Δ_u	maximum displacement corresponding to post-peak load V_u
Δ_y	yield displacement
ϕ_y	curvature at the yield moment
ϕ_u	curvature at the maximum moment
ρ_v	flexural reinforcement ratio
θ_o	drift ratio at maximum load V_{max}
θ_y	yield drift ratio
θ_u	maximum drift ratio corresponding to post-peak load V_u
μ_Δ	displacement ductility ratio

RC walls, which indicates that new methods need to be considered to satisfy the code requirements.

In the present study, new details for emulative PC walls were studied to improve the earthquake performance, particularly ductility and energy dissipation capacity. In contrast to the existing emulative methods that focused on strengthening the PC panel joints, a weakening strategy was used: rebars with partially reduced cross-sectional area were used in the PC panel located at the bottom of the wall so that a plastic hinge zone occurred in the PC panel, preventing brittle failure of the panel joints. To verify the earthquake resistance of the proposed method, four specimens, including a conventional RC wall, were tested under cyclic loading.

2. Proposed methods

In the present study, to prevent gap opening and shear slip at the panel joints of PC walls (see Fig. 1), a weakening strategy based on the capacity design concept [30] was used. The proposed weakening method is conceptually similar to the RBS connection method ([31], [32], etc.), which uses a reduced beam flange section to apply the capacity design concept to moment-resisting steel frames.

Fig. 2a shows the proposed PC wall using unbonded rebars with partially reduced sectional area at the bottom of the wall. Fig. 3a shows the rebar details. The longitudinal rebars are anchored to the splice sleeve embedded in the wall base. At the bottom of the wall, the sectional area is partially reduced, and the length of the reduced portion is unbonded using a PVC pipe. As shown in Fig. 3c, the moment capacity of the wall is determined by the reduced rebar area. Further, by using the unbonded length, early fracture of the rebars and early concrete crushing caused by bond stress can be prevented. Therefore, it is expected that the overall inelastic behavior of the PC wall is governed by the plastic deformation of the unbonded rebars, avoiding gap opening and shear slip at the panel joints. For this purpose, the reduced rebar area should be determined to satisfy the maximum moment demand that is expected to occur at the bottom of the wall. On the basis of the capacity design concept [30–32], the other parts of the wall, including the panel joints, should be designed to have sufficient strengths against the demand forces.

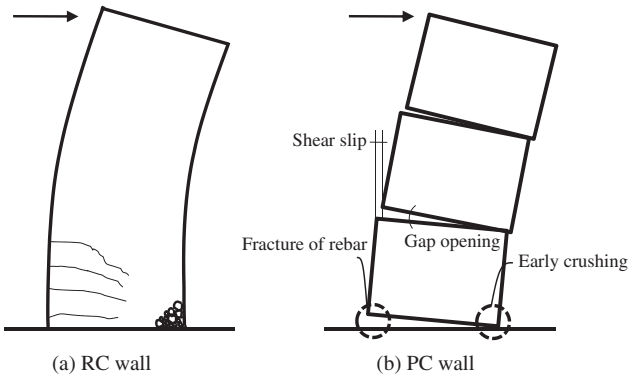

Fig. 1. Failure mode of PC wall.

Fig. 2b shows the proposed method that uses bonded rebars with partially reduced sectional area at the bottom of the wall. Fig. 4a shows the rebar detail, which is similar to the unbonded rebar detail in Fig. 3a. Unlike the unbonded rebar detail, PVC pipe is not used. Nevertheless, because the rebar surface becomes smooth by reducing the rebar sectional area, the length of the reduced rebar area is expected to be unbonded. As shown in Fig. 4c, the moment capacity of the wall is determined by the reduced rebar area.

Fig. 2c shows the proposed RC–PC hybrid wall. The lower part of the wall, where a plastic hinge is expected to develop, is integrated with the wall base using cast-in-place concrete. At the upper levels, ordinary PC panels and connections are used. By using cast-in-place concrete at the bottom of the wall and by maintaining sufficient strengths in the panel joints at the upper levels, the structural performance of the hybrid wall is expected to be equivalent to that of the RC wall.

In the proposed methods, special details are required only at the bottom of the wall. Thus, from the view point of constructability and initial construction cost, the proposed methods have advantages over other existing methods. The RC–PC hybrid method is economically advantageous because no special details are required.

3. Test specimens and setup

Four specimens were tested under cyclic loading. Fig. 5 shows the dimensions and details of the specimens. Fig. 5a–d shows the monolithic RC wall **ST-RC**, the hybrid wall **HY-PC**, the PC wall **BSR-UPC** using unbonded rebars with partially reduced area, and the PC wall **BSR-BPC** using bonded rebars with partially reduced area, respectively. The wall height h from the bottom to the loading

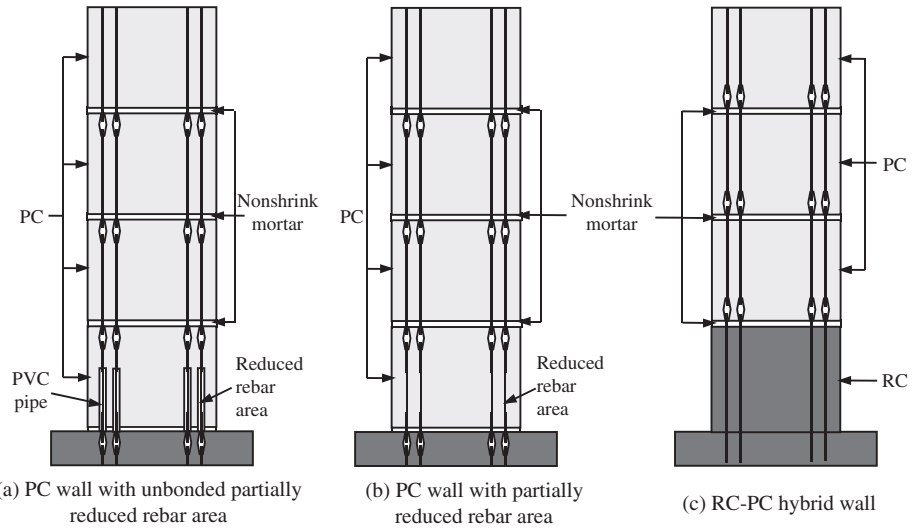

Fig. 2. Proposed PC walls.

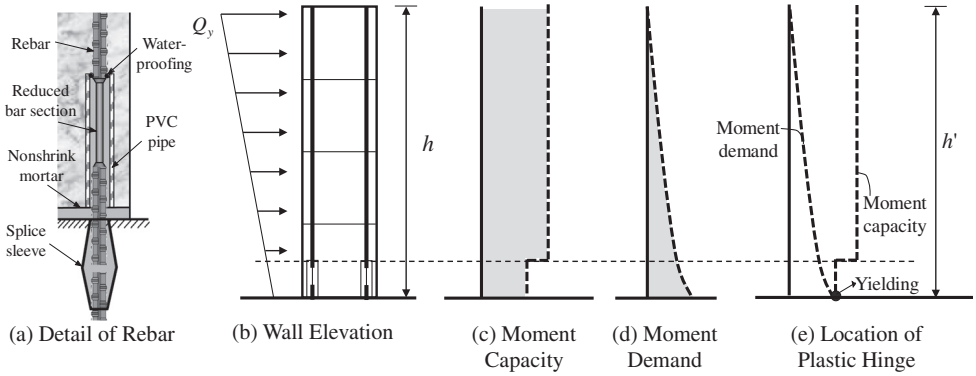

Fig. 3. Proposed method: unbonded rebars with partially reduced sectional area.

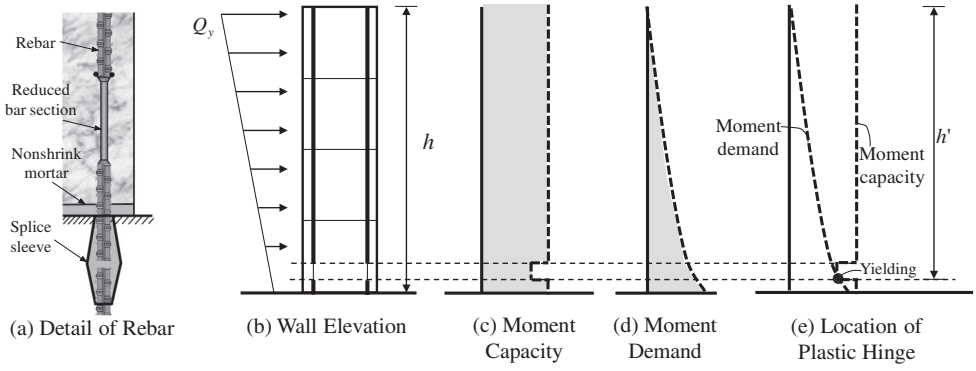

Fig. 4. Proposed method: bonded rebars with partially reduced sectional area.

point was 2000 mm. The wall depth and thickness were 900 mm and 180 mm, respectively. Thus, the aspect ratio of the walls, h/l, was 2.22. For the rebar connection at the PC panel joints, splice-sleeve connections were used. In the splice sleeve connection, top and bottom rebars were inserted into the sleeve, and the sleeve was filled with nonshrink high-strength mortar. To prevent shear-slip failure at the panel joints, shear keys with sufficient shear strength were used. The gap at the panel joints was filled with 20 mm-thick nonshrink high-strength mortar. The concrete compressive strength for specimens **ST-RC**, **HY-PC**, and **BSR-UPC** was 33.6 MPa. The concrete compressive strength for specimen **BSR-BPC** was 32.1 MPa. The compressive strength of the nonshrink mortar was 46.2 MPa. The properties of the rebars used for the specimens are presented in Table 1, and the details of the specimens are shown in Fig. 5.

Fig. 5a shows the RC specimen, **ST-RC**. For the vertical rebars, 16 D13 rebars (Korean standard, bar diameter = 13 mm, area = 127 mm^2, f_y = 434 MPa) were uniformly distributed in two layers. For the horizontal rebars, D10 rebars (bar diameter = 10 mm, area = 71 mm^2, f_y = 555 MPa) were uniformly

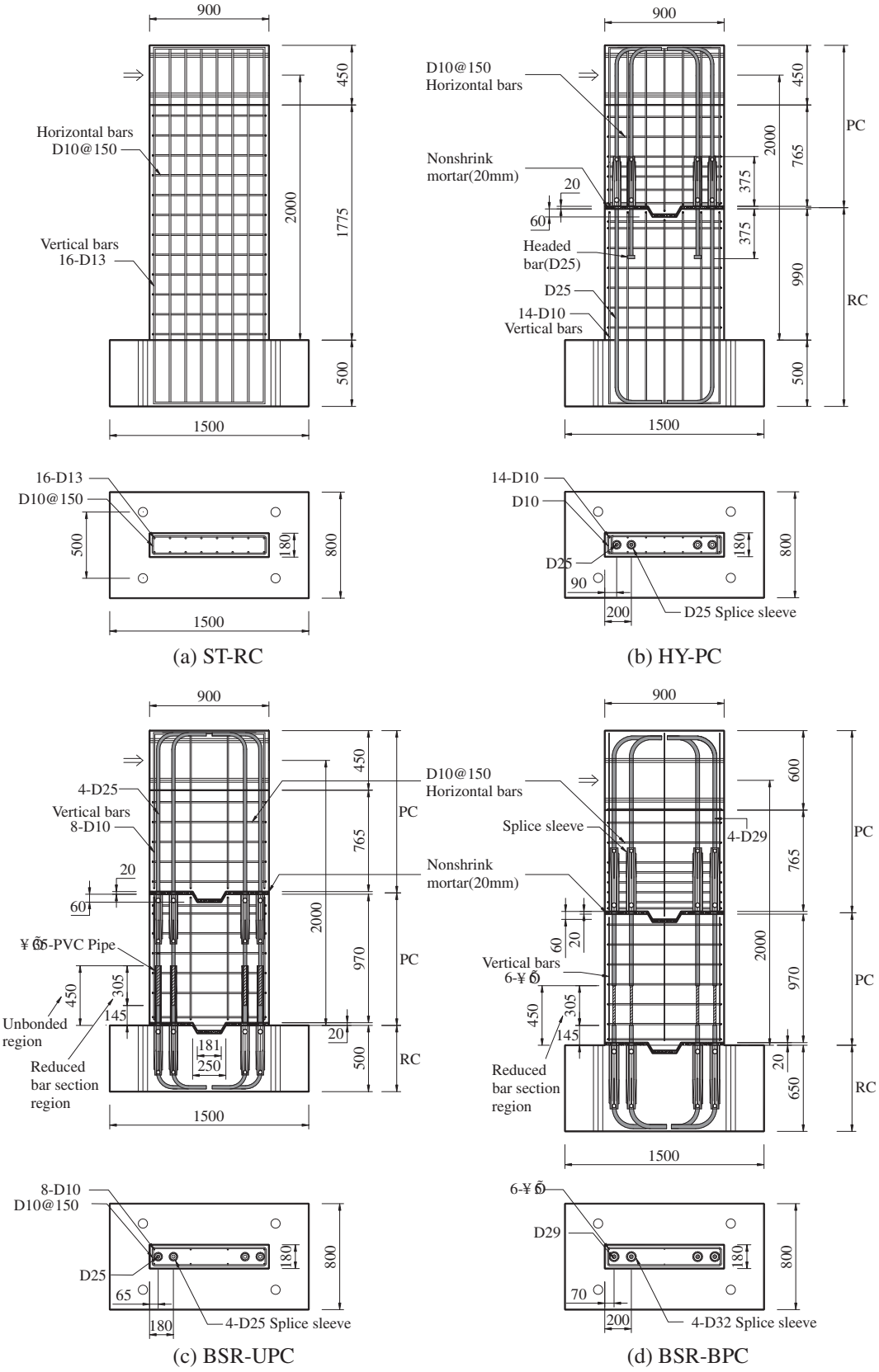

Fig. 5. Test specimens (unit: mm).

distributed in two layers with 150 mm spacing. Fig. 5b shows the hybrid wall **HY-PC**. The height of the cast-in-place concrete panel was 990 mm, and it was connected to the upper PC panel. Two D25 rebars (bar diameter = 25 mm, area = 507 mm^2, f_y = 453 MPa) were continuous through the wall height. Another two D25 headed bars were used to strengthen the RC–PC joint; the headed bars

Table 1
Rebar properties.

	A_s (mm^2)	f_y (MPa)	f_u (MPa)	E_s (MPa)
D10	71	555	675	1.76×10^5
D13	127	434	568	1.83×10^5
D25	507	453	600	1.97×10^5
D29	642	434	490	1.98×10^5

were embedded in the lower RC panel and were sleeve-connected to the rebars in the upper PC panel. At the panel joint, a shear key was used to prevent shear slip. The shear strength at the panel joints was defined as the sum of the shear strength of the shear key and the shear friction strength at the joint based on ACI 318 [29] design code ($V_{pre.(s)}$ in Table 2). In addition to the D25 rebars, 14 D10 rebars were placed in the RC panel. Although the rebar arrangement of the hybrid wall was different from that of the RC wall, the moment-carrying capacity was designed to be the same.

Fig. 5c shows the PC wall **BSR-UPC** using unbonded rebars with partially reduced area. In the wall, four D25 rebars were used for flexural reinforcement. The diameter of the D25 rebars was reduced to 20 mm in the region from 145 mm to 450 mm from the bottom of the wall. The rebars with the reduced area were covered with PVC pipes. The panel joint detail was the same as that used for the **HY-PC** specimen, except for the location of the splice sleeve. Because of the reduced rebar area, the load-carrying capacity of **BSR-UPC** was expected to be less than that of **ST-RC** and **HY-PC**.

Fig. 5d shows the PC wall **BSR-BPC** using bonded rebars with partially reduced area. To maintain a load-carrying capacity equal to that of **ST-RC** and **HY-PC**, a greater bar diameter was used: four D29 rebars (bar diameter = 29 mm, area = 642 mm^2, f_y = 434 MPa). The details of the D29 rebars at the bottom of the wall were similar to those in specimen **BSR-UPC**. The diameter of the D29 rebars was reduced to 24 mm in the region from 145 mm to 450 mm from the bottom of the wall. However, unlike **BSR-UPC** using unbonded rebars, PVC pipes were not used. Thus, at the bottom of the wall, the rebar length with unreduced area (145 mm) was bonded to the concrete, though the rebar length with reduced area (305 mm) was unbonded because of the smooth surface. Other details were similar to those in **BSR-UPC**.

Fig. 6 shows the test setup and loading history. Lateral loading was applied at the top of the wall specimens [33–40]. The loading history was planned according to ACI T1.1R [41] and controlled by displacement. In the case of the **BSR-BPC** specimen, because of an operational error, the loading history was slightly different from that shown in Fig. 6: for target displacement steps, 0.05, 0.1, 0.2, 0.3, 0.45, 0.65, 0.95, 1.4, 2.0, 3.0, and 4.0(%) drift ratios were used. The displacements of the specimens were measured using linear variable differential transformers (LVDT), as shown in Fig. 6. The rebar strains were measured using strain gauges.

4. Test results

4.1. Crack and damage patterns

Fig. 7 shows the concrete crack and damage patterns of the specimens at the end of the test. In the RC wall **ST-RC**, initial flexural cracking occurred at 54 kN (drift ratio = 0.1%), which was approximately 30% of the maximum load. As the lateral displacement increased, initial flexural cracks developed into flexure–shear cracks, proceeding to the center of the wall. Further, new flexural cracks propagated from the wall base to a height of 1700 mm. The failure of the specimen was caused by concrete crushing and rebar fracture in the plastic hinge region of the wall bottom (see Fig. 8a).

In the hybrid wall **HY-PC** specimen, initial flexural cracking occurred at 35.3 kN (drift ratio = 0.05%) at the RC–PC panel joint. Flexural cracking in the lower RC panel first occurred at 39 kN. As the lateral displacement increased, the flexural cracking propagated to the upper PC panel. Ultimately, concrete crushing occurred at the edge of the cross section at the wall bottom, and proceeded to the center of the cross section. The damage pattern was similar to that of the RC specimen. However, in the hybrid

Table 2
Test results.

Specimen		V_y[a] (kN)	V_{max}[b] (kN)	V_u[c] (kN)	Δ_y[d] (mm)	Δ_0[e] (mm)	Δ_u[f] (mm)	θ_y[g] (%)	θ_0[h] (%)	θ_u[i] (%)	μ_Δ[j] (Δ_u/Δ_y)	M_n[k] (kN m)	$V_{pre.}$[l] (kN)	$V_{pre.(s)}$[m] (kN)	$\frac{V_{max}}{V_{pre.}}$[n]	Secant stiffness[o] (kN/mm)
(a) ST-RC	(+)	160.7	179.6	160.8	14.2	55.3	69.4	0.71	2.77	3.47	4.86	343.0	171.5	–	1.05	14.64
	(−)	−156.7	−183.1	−163.8	−13.4	−50.1	−56.2	−0.67	−2.51	−2.81	4.19				1.07	15.26
(b) HY-PC	(+)	187.9	196.4	175.7	14.2	28.5	56	0.71	1.42	2.8	3.94	399.3	199.6	594.7	0.98	16.93
	(−)	−197.9	−202.5	−183.4	−15.7	−46.7	−55.4	−0.78	−2.34	−2.77	3.50				1.01	13.81
(c) BSR-UPC	(+)	133.2	136.7	128.8	12.1	28.3	86	0.60	1.42	4.3	7.11	229.6	114.8	348.5	1.19	16.48
	(−)	−126.3	−131.0	−123.0	−11.9	−16.7	−92	−0.60	−0.84	−4.6	7.73				1.14	16.38
(d) BSR-BPC	(+)	161.0	189.1	186.3	13.2	60.2	60	0.66	3.0	3.0	4.62	307.8	166.4	711.2	1.13	16.02
	(−)	−167.4	−174.4	−170.2	−14.4	−40.0	−60	−0.72	−2.0	−3.0	4.29				1.08	16.07

[a] Yield load.
[b] Maximum lateral load.
[c] Post-peak load corresponding to 90% of V_{max}.
[d] Yield displacement.
[e] Displacement corresponding to maximum lateral load.
[f] Maximum displacement corresponding to post-peak load V_u.
[g] Drift ratio corresponding to yield load.
[h] Drift ratio corresponding to maximum lateral load.
[i] Maximum drift ratio corresponding to post-peak load V_u.
[j] Displacement ductility ratio.
[k] Predicted moment strength at the critical section.
[l] Predicted lateral load strength ($V_{pre.} = M_n/h'$, h' = 2.0 (m) for **ST-RC**, **HY-PC**, and **BSR-UPC**, and h' = 1.85 (m) for **BSR-BPC**; see Figs. 3 and 4).
[m] Predicted shear strength at PC panel joints (the frictional coefficient was assumed to be 0.6).
[n] Ratio of maximum lateral load to predicted lateral load strength.
[o] Secant stiffness corresponding to 0.75V_{max}.

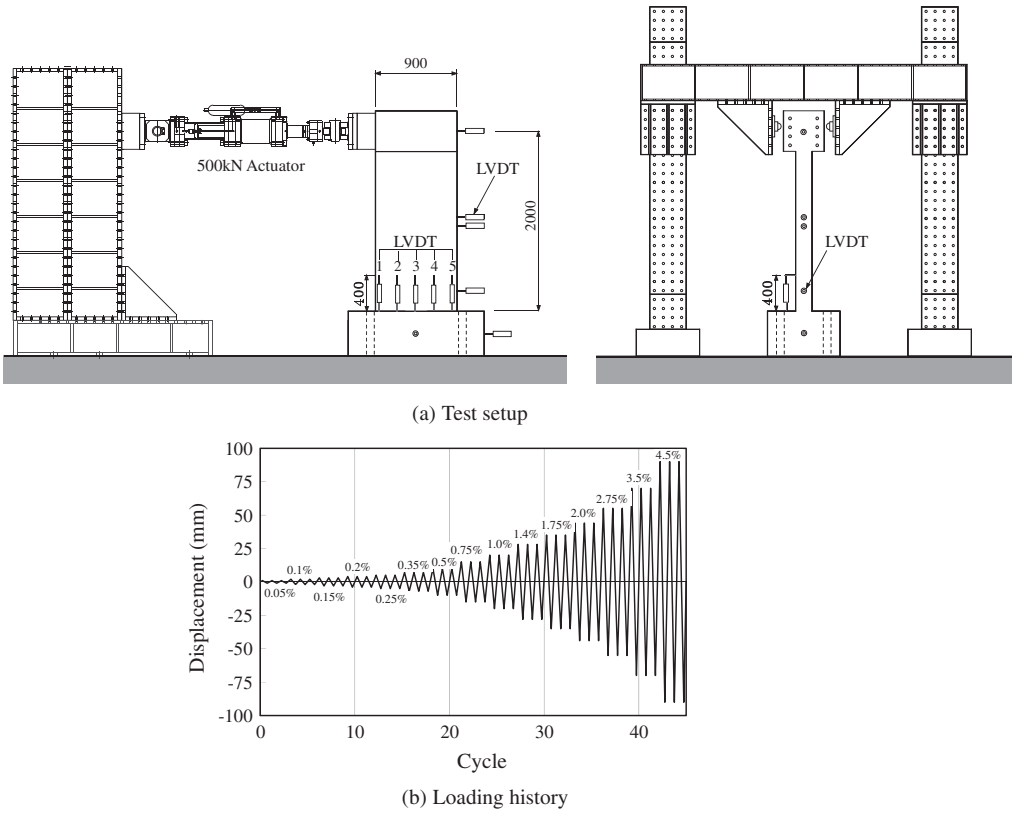

Fig. 6. Test setup and loading history.

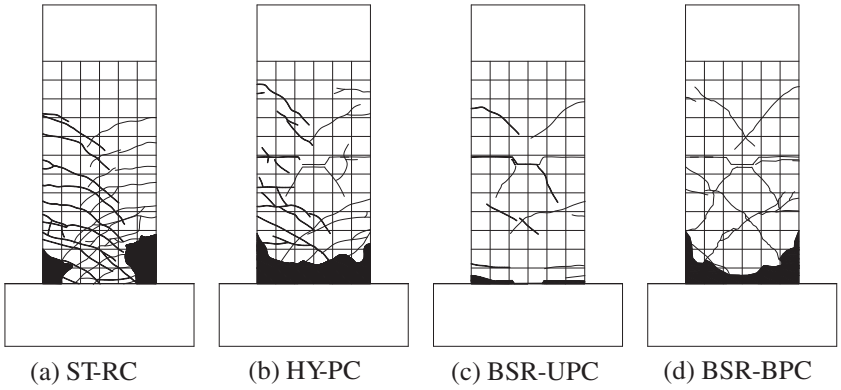

Fig. 7. Crack and damage pattern at the end of the test.

specimen, cracking and concrete crushing were concentrated on the wall bottom, whereas in the RC specimen, concrete cracking was distributed over a larger area of the wall. This is partly because in the hybrid wall, the upper PC panel and the panel joint were designed to have greater flexural strengths to avoid failure of the panel joint.

In the PC wall **BSR-UPC**, initial flexural cracking occurred at 27.8 kN (drift ratio = 0.05%) at the panel-to-base joint. Flexural cracking at the PC panel-to-panel joint occurred at 31.2 kN. Additional flexural cracks occurred until the lateral drift reached 0.5%. After this lateral drift, no further cracks occurred and only existing cracks propagated. When the displacement drift reached 1%, the nonshrink mortar at the panel-to-base joint started to be crushed and the tensile strain of the rebars with reduced area increased significantly, exceeding the yield strain. Until a 4.5% drift ratio was reached, no severe damage occurred in the PC panels, and concrete crushing at the panel-to-base joint proceeded gradually (Fig. 8b). At 4.5% drift, the test came to an end because the actuator reached the stroke limitation. However, the strength of the specimen did not decrease at the 4.5% lateral drift ratio.

In the **BSR-BPC** specimen, initial flexural cracking occurred at 51 kN (drift ratio = 0.1%) at the panel-to-base joint. Flexural cracking in the PC panel with a reduced rebar area first occurred at 67 kN. Additional flexural cracking occurred at the PC panel-to-panel joint. After the yielding of the rebars with reduced area, only the existing cracks propagated, and no further cracking occurred. Ultimately, concrete crushing occurred at the wall bottom.

As shown in Fig. 7, in specimen **BSR-UPC**, significant crushing and cracking did not occur in the concrete. This result showed that the overall deformation of the wall was governed by the deformation of the unbonded rebars with reduced sectional area.

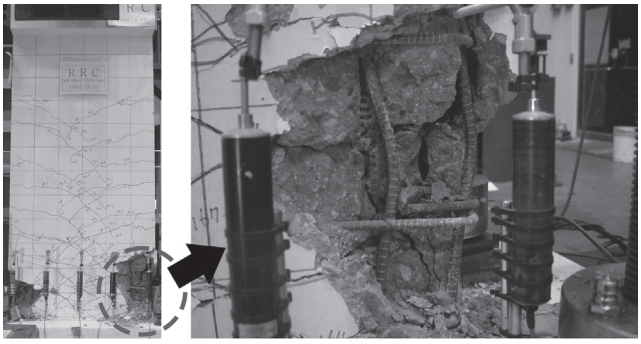

(a) ST-RC

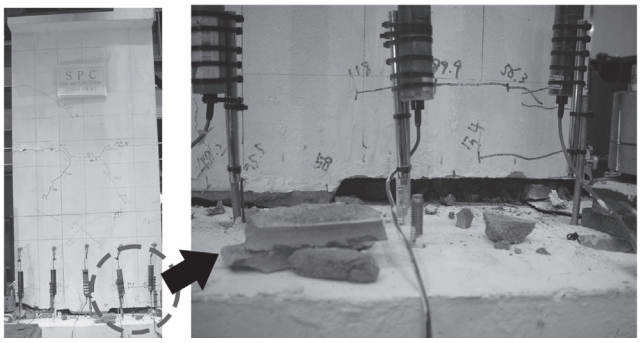

(b) BSR-UPC

Fig. 8. Detailed damage pattern at failure.

4.2. Lateral load–drift ratio relationship

Fig. 9 shows the lateral load–drift ratio relationship of the specimens. Table 2 summarizes the test results, including the maximum load V_{max} and the maximum drift ratio θ_u. The maximum drift ratio θ_u was defined as the post-peak drift ratio corresponding to 90% of the maximum load V_u (=0.9V_{max}). In the **ST-RC** specimen, the maximum load V_{max} reached 179.6 kN at +2.77% drift ratio. After the maximum loading, the load carrying capacity gradually decreased. The maximum drift ratio θ_u was −2.81%. The maximum load of the **HY-PC** specimen was 196.4 kN (at +1.42% drift ratio), which was greater than that of the RC specimen. The maximum drift ratio was −2.77%. The maximum load of the PC wall **BSR-UPC** was 131 kN (at −0.84%), which was less than the maximum load of **ST-RC** and **HY-PC** as a result of the reduced rebar area. Unlike the other specimens, significant strength-degradation did not occur during cyclic loading. The maximum drift ratio was +4.3%. The maximum load of the **BSR-BPC** specimen was 174.4 kN (at −2% drift ratio). The maximum drift ratio was 3.0%.

As shown in the test results, the PC wall **BSR-UPC** and **BSR-BPC** specimens using the proposed weakening strategy exhibited good deformation capacities that were equivalent to or greater than that of the RC specimen. This result demonstrates the validity of the proposed rebar details using rebars with reduced sectional area. Particularly, in the **BSR-UPC** specimen, significant stiffness- and strength-degradations did not occur during cyclic loadings. In contrast, in the other specimens, strength degradation occurred as the number of repeated cyclic loadings increased. This result indicates that the unbonded rebar detail with reduced rebar area was effective in preventing cyclic strength degradation.

4.3. Strength, stiffness, displacement ductility, and energy dissipation capacity

In Fig. 9 and Table 2, the predicted lateral load $V_{pre.}$ was compared with the test results, V_{max}. $V_{pre.}$ was calculated from

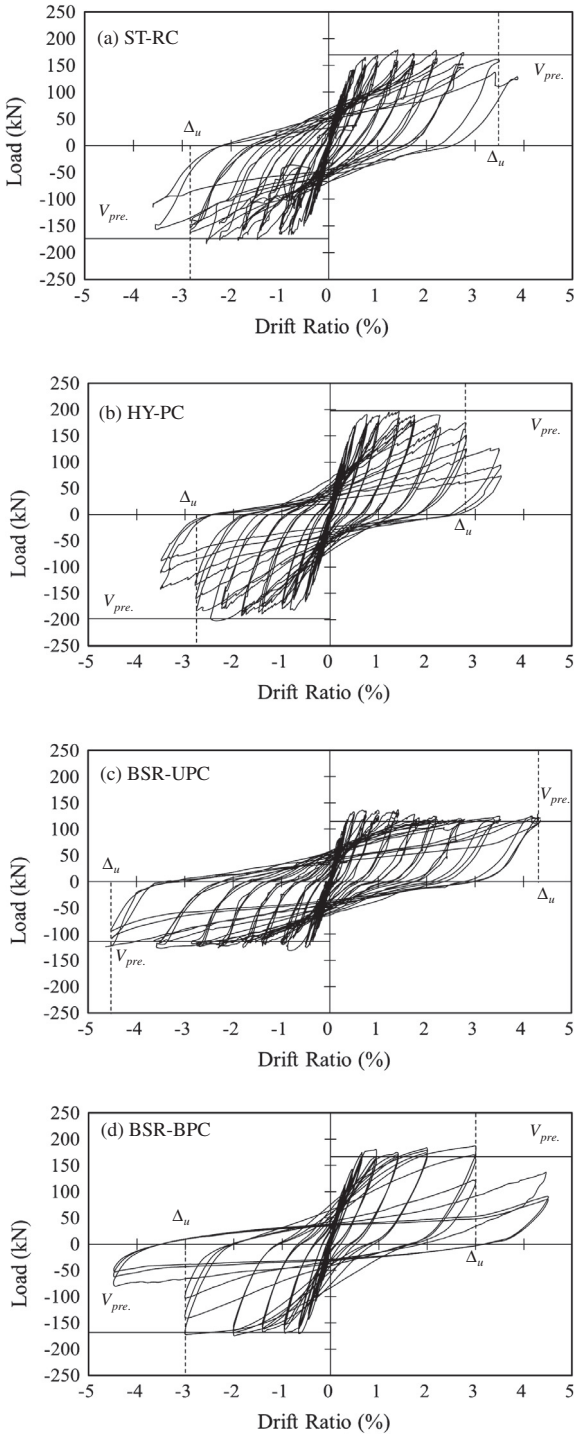

Fig. 9. Load–drift ratio relationship.

the moment capacity (M_n) at the flexural critical section: $V_{pre.} = M_n/h'$ (see Figs. 3 and 4 for the effective height h'). The moment capacity (M_n) at the flexural critical section was calculated using the reduced rebar section (see Section 4.4). To prevent undesirable shear failure at the PC panel joints, the shear strength of the PC panel joints $V_{pre.(s)}$ was designed to be greater than $V_{pre.}$ (Table 2). $V_{pre.(s)}$ was calculated as the sum of the contributions of shear key and shear friction. In Table 2, the $V_{max}/V_{pre.}$ ratios for all specimens were close to 1.0, which indicates that the predicted maximum loads agreed well with the test results.

In Table 2, the secant stiffness was defined as the value corresponding to 75% of the maximum load. Since the strength of

specimen **BSR-UPC** was the smallest, the load corresponding to the secant stiffness point was also the smallest. Thus, the degradation of the secant stiffness due to concrete damage was less in **BSR-UPC**. For this reason, **BSR-UPC** showed the greatest secant stiffness. However, the difference was not significant. Generally, the secant stiffness of the proposed PC walls was comparable to that of specimen **ST-RC**.

In Table 2, the displacement ductility μ_Δ (= Δ_u/Δ_y) was evaluated. The maximum Δ_u was defined as the post-peak displacement corresponding to $0.9V_{max}$. The yield load V_y and displacement Δ_y were defined by the offset method [42]: The yielding load V_y was defined at the intersection of the lateral load–drift envelope curve and the initial slope starting from a 0.3% drift offset point. The displacement ductility μ_Δ of the hybrid wall **HY-PC** was 3.50, which was less than that of **ST-RC** (μ_Δ = 4.19). The displacement ductility values of the PC walls **BSR-UPC** and **BSR-BPC** were 7.11 and 4.29, respectively, which were equivalent to or greater than that of **ST-RC**.

Fig. 10a and b shows the energy dissipation per drift ratio and the cumulative energy dissipation. The energy dissipation per drift ratio indicates the area enclosed by a load cycle. Fig. 10c shows the energy dissipation at the 3rd load cycle at each drift ratio, which represents the energy dissipation degraded by repeated cyclic loading. The specimens' performance can be more clearly compared by the equivalent damping ratio β_o [43] (= $E_D/4\pi E_{so}$) which represents the normalized energy dissipation capacity (Fig. 10d). In the comparisons, the specimen **BSR-BPC** was excluded because of the different loading history. As shown in the figures, the specimens **HY-PC** and **BSR-UPC** exhibited good energy dissipation that was comparable to or better than that of the RC specimen. The specimen **BSR-UPC** exhibited the best energy dissipation capacity among the specimens.

Fig. 11 shows the vertical strain distributions at the wall bottom which were measured by LVDT 1 through LVDT 5 in Fig. 6a. The vertical strain indicates the average value for a length of 400 mm at the wall bottom. As shown in Fig. 11, the vertical strains tended to increase as the drift ratio increased. In the **BSR-UPC** specimen, only tensile strains occurred over the entire cross section after 0.75% drift ratio (Fig. 11c). When reinforced concrete members with no or moderate axial load is subjected to cyclic transverse loading, member elongation occurs due to the plastic strain of the flexural rebars [44] (see Fig. 12). As the axial compressive load increases, member elongation decreases. The tensile strain in **BSR-UPC** was the greatest, which indicates that the plastic hinge deformation was more concentrated at the wall bottom, and the majority of the overall deformation of the wall was developed by the inelastic deformation of the unbonded rebars with reduced area. Fig. 12 also demonstrates the large inelastic deformations of the rebars during cyclic loading.

Regarding the strain distribution of specimen **ST-RC** (Fig. 11a), the strain of the first LVDT from the tensional boundary decreased as the loading cycle proceeded because the tensional crack and deformation shifted upward and it was located out of the measurement range of the first LVDT from the tensional boundary (Figs. 7 and 8a).

4.4. Moment–curvature relationship

Fig. 13 shows the moment–curvature relationships at the wall bottom, obtained from the test results and the prediction. From the test results, the moment capacity was estimated at the critical section. The curvature was estimated by dividing the differential strain between the LVDT 1 and LVDT 5 by the horizontal distance 800 mm (see Figs. 6a and 11). When calculating the curvature of specimen **ST-RC**, because of the decrease in strain at the tensional boundary, the strain of the second LVDT from the tensional boundary and the horizontal distance of 600 mm between the LVDTs were used.

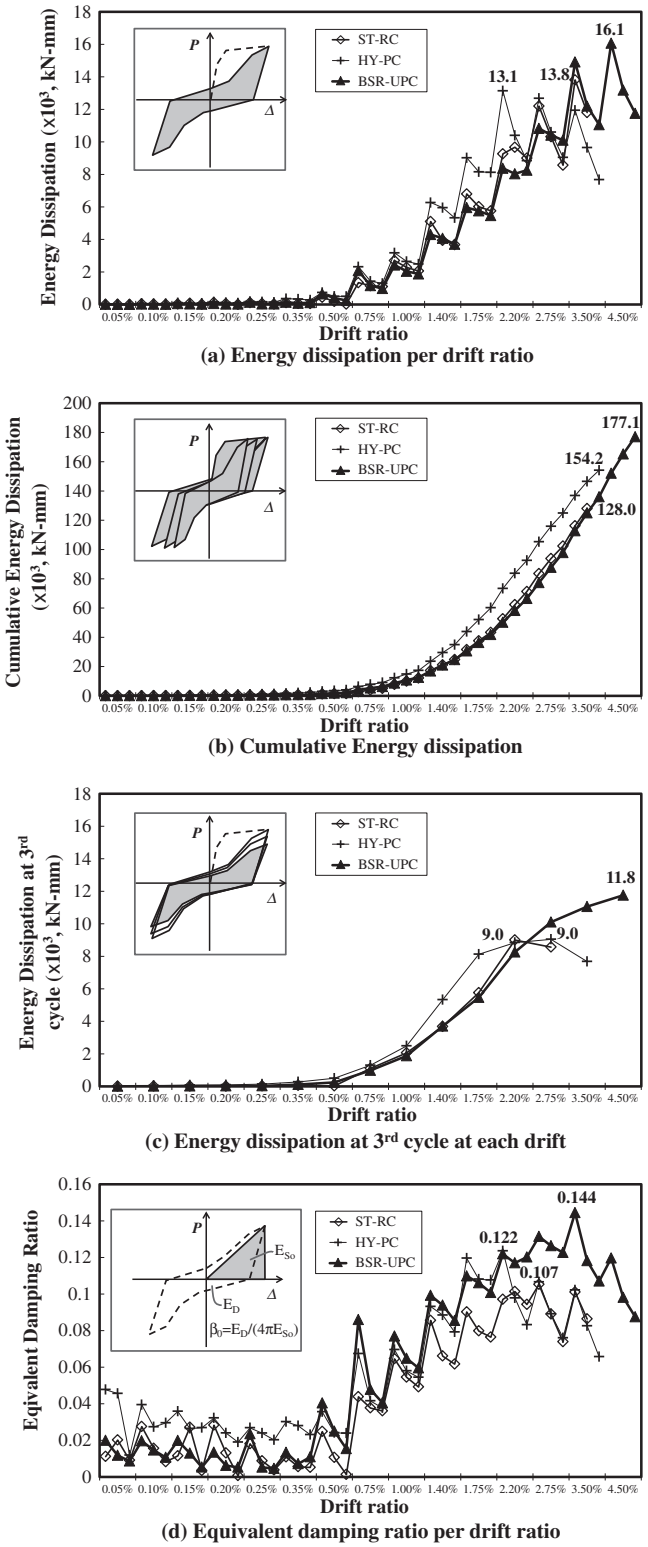

Fig. 10. Energy dissipation of test specimens.

In the predictions, the yield moment–curvature and the maximum moment–curvature were calculated (Fig. 14). According to FEMA 273 [45] (Fig. 14a), the yield moment point was defined as the time when the strain at 0.25l from the tension end reaches the yielding strain ε_y of the rebar (Fig. 14a). The ultimate point

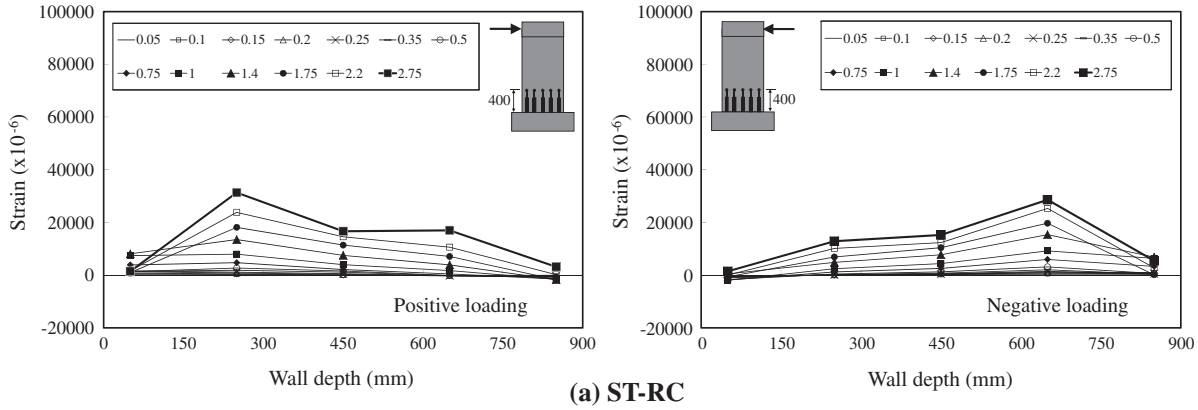

(a) ST-RC

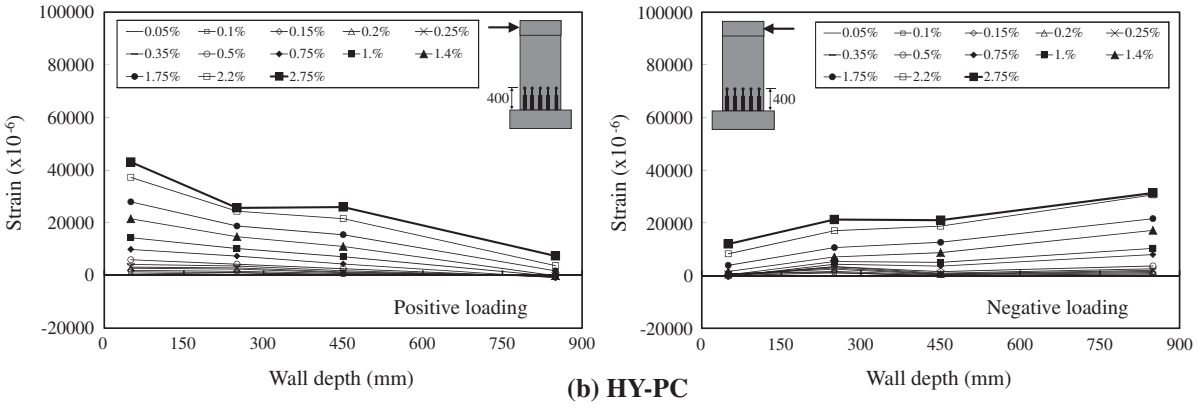

(b) HY-PC

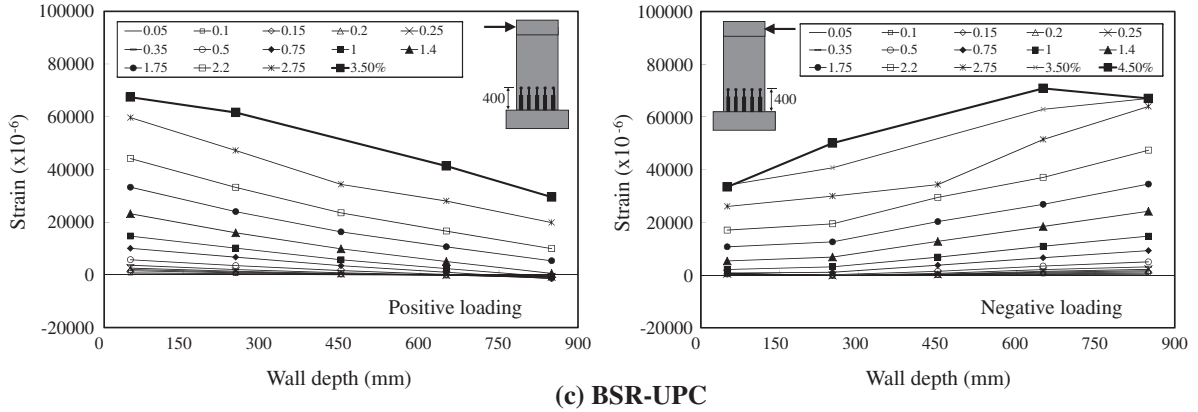

(c) BSR-UPC

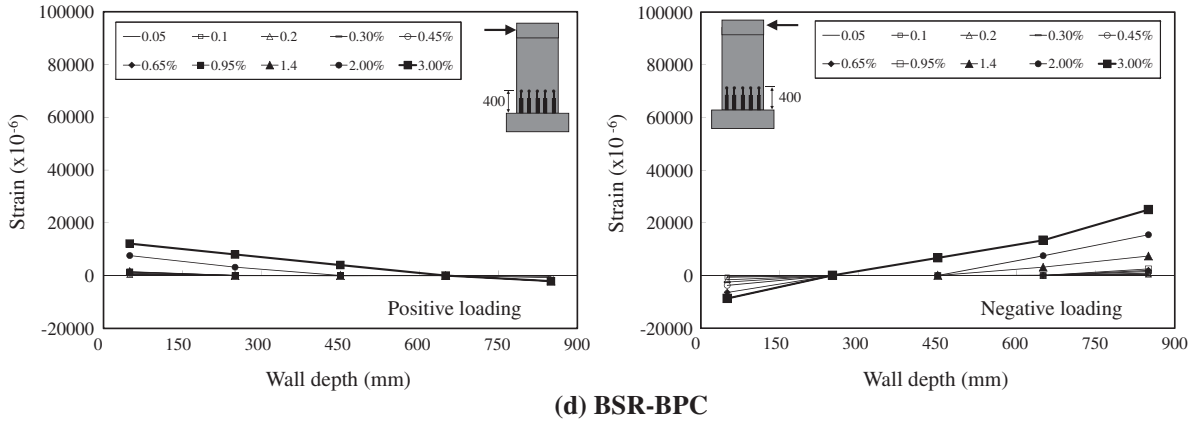

(d) BSR-BPC

Fig. 11. Vertical strain distribution at the wall bottom.

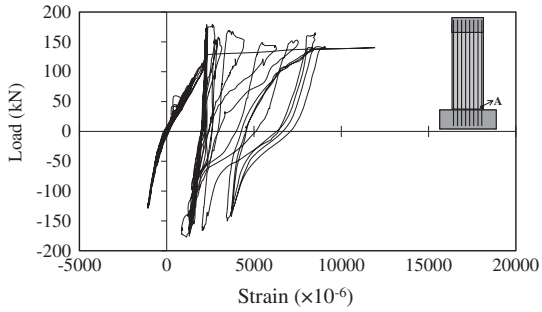

(a) ST-RC

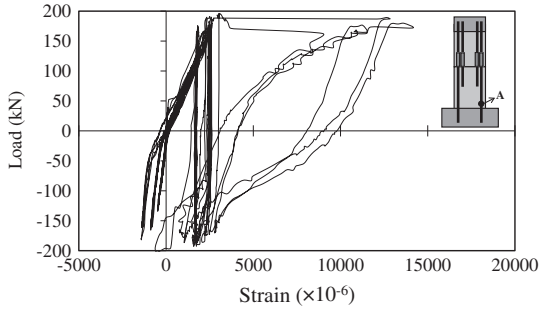

(b) HY-PC

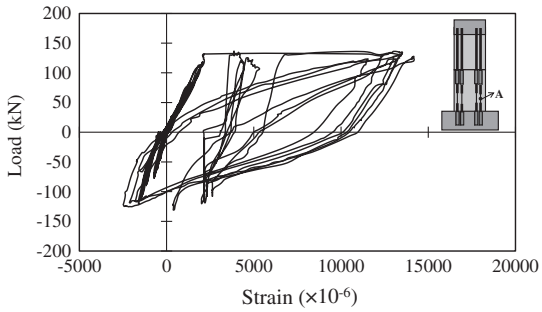

(c) BSR-UPC

Fig. 12. Cyclic stress–strain relationship of rebars at the critical section (region A).

(i.e. maximum moment point) was defined as the time when the strain of the compression end reaches the ultimate strain of the concrete, 0.004 [46–50] (Fig. 14b). Using the linear strain distribution in Fig. 14a and b which is generally used for the calculation of flexural strength of RC structural member, the curvature and moment at the yield moment point and the maximum moment point were calculated. The curvature ϕ_y and moment M_y at the yield moment point was defined as below Eqs. (1) and (2) and the curvature ϕ_u and moment M_u at the maximum moment point was defined as below Eqs. (3) and (4). Detailed calculation process was introduced in previous studies [47,48,50,51].

$$\phi_y = \frac{\varepsilon_y}{0.75l - c_y} \tag{1}$$

$$M_y = C_c\left(\frac{l}{2} - \frac{c_y}{3}\right) + \sum_{k=1}^{n}\left(x_k - \frac{l}{2}\right)A_{sk}f_{sk} \tag{2}$$

where C_c = compression force of concrete = $0.5E_c\varepsilon_c c_y t$, ε_c = strain of the compression end, c_y = depth of compression zone at yield moment, t = wall thickness, E_c = elastic modulus of concrete, A_{sk} = section area of rebar, and f_{sk} = stress of rebar ($-f_y \leqslant f_{sk} \leqslant f_y$).

$$\phi_u = \frac{0.004}{c} \tag{3}$$

$$M_u = C_c\left(\frac{l}{2} - \frac{\beta c_u}{2}\right) + \sum_{k=1}^{n}\left(x_k - \frac{l}{2}\right)A_{sk}f_{sk} \tag{4}$$

where $C_c = \alpha\beta f_c' c_u t$, c_u = depth of compression zone at the maximum moment and α, β = coefficients corresponding to a rectangular stress block of the concrete.

As shown in Fig. 13, the predicted yield moments were slightly less than the test results, whereas the maximum moments agreed with the test results. In the case of curvature, the predicted ultimate curvatures were a little less than the test results. This result showed that, the strength and deformation of the proposed wall systems can be safely predicted by conventional methods using linear strain distribution and concrete crushing strain.

The depth of the compression zone at the maximum moment was calculated from the stress and strain distributions shown in Fig. 14b. The results are presented in Table 3. Generally, the compression zone depth is proportional to the reinforcement ratio and axial load [47–49]. This trend was shown in Table 3: Specimen **BSR-UPC** with the lowest reinforcement ratio showed the smallest compression zone depth and the greatest curvature. This result indicates that the good deformation capacity of **BSR-UPC** was caused by the low reinforcement ratio as well as the proposed detail using unbonded reduced rebar area.

The deformation capacities resulting from this test were those for the walls without axial force. If axial compressive force is applied and the reinforcement ratio increases, the deformation capacity of such walls should be evaluated considering the increase of the compression zone depth.

5. Discussion and further research

In this proposed PC wall, the reduced rebar area should be carefully determined to satisfy the purpose of capacity design. It should be determined to resist the moment demand at the intended plastic hinge region that is generally located at the wall bottom. By using the concept of capacity design [30–32], the other parts of the wall, including the panel joints, are designed to have sufficient strength against the demand forces. This capacity design concept for the proposed PC wall can be expressed as Eq. (5).

$$\left(\frac{M_{capacity}}{M_{demand}}\right) \text{ at intended plastic hinge} < \left(\frac{M_{capacity}}{M_{demand}}\right) \text{ at the other parts} \tag{5}$$

As shown in the Section 4.4, conventional methods using linear strain distribution and concrete crushing strain [47–51] can be used to determine the strength ($M_{capacity}$) of the intended plastic hinge region at the design procedure of the proposed PC wall: Eq. (4) can be used for determining the moment strength capacity ($M_{capacity}$) at the intended hinge region. Therefore, the reduced rebar area can be determined by using Eqs. (4) and (5) based on capacity design concept.

However, the reduced rebar area may be limited. If the reduction was excessive, premature buckling and/or fracture of the rebars may occur [52,53]. As shown in Table 3, the flexural rebar reinforcement ratio of each specimen at the critical section is greater than the minimum requirement 0.0015 by ACI 318-08 [29], therefore all the specimens behaved stably under lateral cyclic loading. Apart from the minimum reinforcement requirement by design code, according to the study conducted by Wood [52,53], the flexural reinforcement ratio (ρ_v) should be limited by Eq. (6) to protect premature buckling and/or fracture of the flexural rebars under cyclic lateral loading.

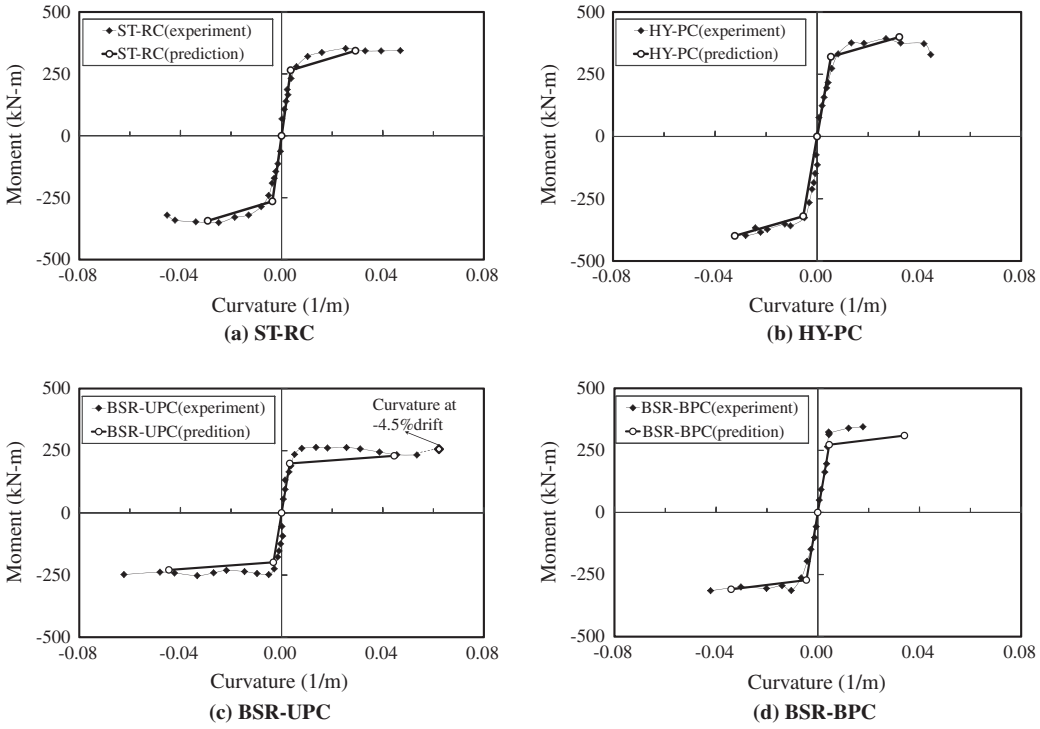

Fig. 13. Moment–curvature relationship from test results and prediction.

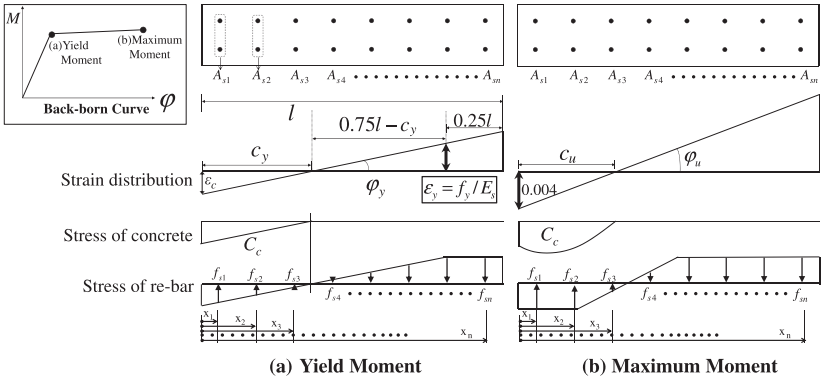

Fig. 14. Stress and strain distributions for predictions of yield moment and maximum moment.

$$\left(\frac{\rho_v f_y + P/A}{f_c'}\right) > 0.15 \tag{6}$$

The Eq. (6) can be used to limit the reduced rebar area in the proposed PC wall. However further study was needed to verify the applicability of Eq. (6) to the proposed PC wall system because the differentiated rebar detail was used in the proposed PC wall. Including this aspect, the following additional researches are still required to further verify the performance of the proposed PC wall details.

In case of **BSR-UPC** or **BSR-BPC**, if the reduced rebar area increases, premature buckling and/or fracture of the rebars may occur [52,53]. Thus, the limitations of reduced rebar area should be studied.

Because the load-carrying capacity of specimen **BSR-UPC** was less than those of other specimens owing to the low reinforcement ratio, the details of unbonded reduced rebar area should be verified further, particularly for the deformation capacity.

Because the proposed method has no ability of "self-centering," and the unbonded rebars are embedded in the PC panel, the pro-

Table 3
Compression zone depth and curvature at maximum moment.

Specimen	ρ_v, Reinforcement ratio[a]	c, Length of compression zone at ultimate state (mm)	φ_u, Ultimate curvature by Eq. (3) (1/m)
(a) **ST-RC**	0.0125	137	0.0292
(b) **HY-PC**	0.0092	124	0.0323
(c) **BSR-UPC**	0.0078	90	0.0445
(d) **BSR-BPC**	0.0121	117	0.0341

[a] Vertical rebar reinforcement at critical section. Reduced bar section was considered. All reinforcement ratios were greater than minimum requirement 0.0015 by ACI 318-08 [1].

posed method is not a good choice when retrofitting is required. Therefore, the proposed details should be improved for situations where retrofitting is frequently needed.

6. Conclusions

In the present study, new details were investigated to enhance the ductility and energy dissipation capacity of emulative PC walls. Unlike the existing studies using strengthening methods, a weakening method was employed in this study. By using bonded or unbonded rebars with partially reduced area at the wall bottom, plastic hinging was introduced in the PC panel rather than at the panel joint. A hybrid wall was also studied, using cast-in-place concrete for the potential plastic hinge region at the wall bottom. On the basis of the capacity design concept, the PC panel joints were designed to have sufficient strengths to prevent the joint failure. To verify the proposed method, four specimens were tested: conventional RC wall, hybrid wall **HY-PC**, PC wall **BSR-UPC** using unbonded reduced rebar area, and PC wall **BSR-BPC** using bonded reduced rebar area. The results of the present study are summarized as follows.

(1) The strength, stiffness, displacement ductility, and energy dissipation capacity of the specimens **HY-PC**, **BSR-UPC**, and **BSR-BPC** were comparable to those of the RC wall. This result indicates that the proposed wall details successfully prevented gap opening and shear slip at the panel joints, on the basis of the capacity design concept.
(2) The PC wall **BSR-UPC** using the unbonded reduced rebar area exhibited the best energy dissipation and deformation capacity. Further, stiffness- and strength-degradations were minimized during cyclic loading. However, because **BSR-UPC** had the lowest reinforcement ratio (deformation capacity tends to be inversely proportional to the reinforcement ratio), the proposed details using unbonded reduced rebar area should be verified further.
(3) In specimen **BSR-UPC**, unlike the other specimens, significant crushing and cracking damage did not occur in the concrete. This result indicates that the overall deformation of the wall was governed by the inelastic deformation of the unbonded rebars with reduced area.
(4) The strength and deformation capacity of the test specimens were adequately predicted by conventional design methods based on linear strain distribution and concrete crushing strain 0.004.
(5) Further studies are required on the effect of axial load, limitation of the reduced rebar area, possibility of premature buckling and/or fracture of rebars, and the applicability to seismic retrofit.

Acknowledgement

This research was financially supported by The Ministry of Construction & Transportation of Korea (05 D02-1). This financial support is gratefully acknowledged.

References

[1] Mueller P. Experimental investigation on the seismic performance of precast wall. In: Ninth world conference on earthquake engineering, Tokyo-Kyoto, Japan; 1988. p. 755–60.
[2] Olivia M, Clough R, Malhas F. Seismic behavior of large panel precast concrete walls: analysis and experiment. PCI J 1989;34(5):42–66.
[3] Hutchinson R, Rizkalla S, Lau M, Heuvle S. Horizontal post-tensioned connections for precast concrete load-bearing shear wall panels. PCI J 1991;36(6):64–76.
[4] Priestley MJN. Overview of PRESSS research program. PCI J 1991;36(4):50–7.
[5] Priestley MJN, Sritharan S, Conley JR, Pampanin S. Preliminary results and conclusions from the PRESSS five-storey precast concrete test buildings. PCI J 1999;44(6):42–67.
[6] Kurama Y, Sause R, Pessiki S, Lu LW. Lateral load behaviour and seismic design of unbonded post-tensioned precast concrete walls. ACI Struct J 1999;96(4):622–32.
[7] Kurama Y, Pessiki S, Sause R, Lu LW. Seismic behavior and design of unbonded post-tensioned precast concrete walls. PCI J 1999;44(3):72–89.
[8] Kurama Y. Seismic design of unbonded post-tensioned precast concrete walls with supplemental viscous damping. ACI Struct J 2000;97(4):648–58.
[9] Rahman A, Restrepo JI. Earthquake resistant precast concrete building: seismic performance of cantilever walls prestressed using unbonded tendons. Research rep no 2000–5. Dept of Civil Engineering, Univ of Canterbury, Christchurch, New Zealand; 2000.
[10] Kurama Y. Seismic response evaluation of unbonded post-tensioned precast walls. ACI Struct J 2002;99(5):641–51.
[11] Holden T, Restrepo J, Mander JB. Seismic performance of precast concrete and prestressed concrete walls. J Struct Eng, ASCE 2003;129(3):286–96.
[12] Seo C, Sause R. Ductility demands on self-centering systems under earthquake loading. ACI Struct J 2005;102(2):275–85.
[13] Kurama Y. Seismic design of partially post-tensioned precast concrete walls. PCI J 2005;55(4):100–25.
[14] Turmo J, Ramos G, Aparicio AC. FEM modelling of unbonded post-tensioned segmental beams with dry joints. Eng Struct 2006;28(13):1852–63.
[15] Wiebe L, Christopoulos C. Mitigation of higher mode effects in base-rocking systems by using multiple rocking sections. J Earthq Eng 2008;13(S1):83–108.
[16] Aaleti S, Sritharan S. A simplified analysis method for characterizing unbonded post-tensioned precast wall systems. Eng Struct 2009;31(12):2966–75.
[17] Smith B, Kurama Y. Seismic behavior of a hybrid precast concrete wall specimen: measured response versus design predictions. In: Joint 9USN/10CCEE conference proceedings, Toronto, Canada; July 25–29, 2010. p. 348–57.
[18] Vasdravellis G, Karavasilis TL, Uy B. Finite element models and cyclic behavior of self-centering steel post-tensioned connections with web hourglass pins. Eng Struct 2013;52:1–16.
[19] Chou CC, Chang HJ, Hewes JT. Two-plastic-hinge and two dimensional finite element models for post-tensioned precast concrete segmental bridge columns. Eng Struct 2013;46:205–17.
[20] Cheng CT. Shaking table tests of a self-centering designed bridge substructure. Eng Struct 2008;30(12):3426–33.
[21] Shim CS, Chung CH, Kim HH. Experimental evaluation of seismic performance of precast segmental bridge piers with a circular solid section. Eng Struct 2008;30(12):3782–92.
[22] Karavasilis TL, Seo CY. Seismic structural and non-structural performance evaluation of highly damped self-centering and conventional systems. Eng Struct 2011;33(8):2248–58.
[23] Chou CC, Chen JH. Analytical model validation and influence of column bases for seismic responses of steel post-tensioned self-centering MRF systems. Eng Struct 2011;33(9):2628–43.
[24] Miller DJ, Fahnestock LA, Eatherton MR. Development and experimental validation of a nickel–titanium shape memory alloy self-centering buckling-restrained brace. Eng Struct 2012;40:288–98.
[25] Bai L, Zhang Y. Nonlinear dynamic behavior of steel framed roof structure with self-centering members under extreme transient wind load. Eng Struct 2013;49:819–30.
[26] Soudki KA. Behavior of horizontal connections for precast concrete load-bearing shear wall panels subjected to large reversed cyclic deformations. PhD thesis. University of Manitoba, Winnipeg, Manitoba; 1994.
[27] Soudki KA, Rizkalla SH, LeBlanc B. Horizontal connections for precast concrete shear walls subjected to cyclic deformations. Part 1: mild steel connections. PCI J 1995;40(4):78–97.
[28] Han J. An experimental study on dry-connections for precast concrete walls. Master's degree. Seoul National University, Seoul, Korea; 2005.
[29] American Concrete Institute. Building code requirements for structural concrete and commentary (ACI 318-08); 2008.
[30] Park R, Paulay T. Reinforced concrete structures. New York, USA: John Wiley & Sons, Inc.; 1975.
[31] Iwankiw N. Ultimate strength consideration for seismic design of the reduced beam section (internal plastic hinge). Eng J, Am Inst Steel Constr 1997;First quarter:3–16.
[32] Englehardt MD, Winneberger T, Zekany AJ, Potyraj TJ. Experimental investigation of dogbone moment connections. Eng J, Am Inst Steel Constr 1997;Fourth quarter:12.1–21.
[33] Riva P, Meda A, Giuriani E. Cyclic behaviour of a full scale RC structural wall. Eng Struct 2003;25(6):835–45.
[34] Greifenhagen C, Lestuzzi P. Static cyclic tests on lightly reinforced concrete shear walls. Eng Struct 2005;27(11):1703–12.
[35] Su RKL, Wong SM. Seismic behaviour of slender reinforced concrete shear walls under high axial load ratio. Eng Struct 2007;29(8):1957–65.
[36] Dazio A, Buzzini D, Trüb M. Nonlinear cyclic behaviour of hybrid fibre concrete structural walls. Eng Struct 2008;30(11):3141–50.
[37] Dazio A, Beyer K, Bachmann H. Quasi-static cyclic tests and plastic hinge analysis of RC structural walls. Eng Struct 2009;31(7):1556–71.
[38] Karamlou A, Kabir MZ. Experimental study of L-shaped slender R-ICF shear walls under cyclic lateral loading. Eng Struct 2012;36:134–46.

[39] Dan D. Experimental tests on seismically damaged composite steel concrete walls retrofitted with CFRP composites. Eng Struct 2012;45:338–48.
[40] Quiroz LG, Maruyama Y, Zavala C. Cyclic behavior of thin RC Peruvian shear walls: full-scale experimental investigation and numerical simulation. Eng Struct 2013;52:153–67.
[41] American Concrete Institute. Commentary on acceptance criteria for moment frames based on structural testing (ACI T1.1R-01); 2001.
[42] Lee E. Shear behavior of hybrid connection consisted of reinforced concrete column and steel beam. PhD thesis. Hanyang University, Seoul, Korea; 2005.
[43] ATC. Seismic evaluation and retrofit of concrete buildings (ATC-40). Applied Technology Council, Redwood City, California; 1996.
[44] Eom TS, Park HG. Evaluation of energy dissipation of slender reinforced concrete members and its applications. Eng Struct 2010;32(9):2884–93.
[45] Building Seismic Safety Council. NEHRP guidelines for the seismic rehabilitation of buildings (FEMA, report 273); 1997.
[46] Paulay T, Priestley MJN. Seismic design of reinforced concrete and masonry buildings. Wiley Interscience; 1992.
[47] Wallace JW. A new methodology for seismic design of reinforced concrete shear walls. J Struct Eng, ASCE 1994;120(3):863–84.
[48] Thomsen JH, Wallace JW. Displacement-based design of RC structural wall: an experimental investigation of walls with rectangular and T-shaped cross-sections. Report no Cu/Cee-95-06. Department of civil and environmental Engineering at Clark University, USA; 1995.
[49] Cho BH. Deformation based seismic design of asymmetric wall structures. PhD thesis. Seoul National University, Seoul, Korea; 2002.
[50] Tjhin TN, Aschheim MA, Wallace JW. Yield displacement-based seismic design of RC wall buildings. Eng Struct 2007;29(11):2946–59.
[51] Park HG, Kang SM, Chung L, Lee DB. Moment–curvature relationship of flexure-dominated walls with partially confined end-zones. Eng Struct 2007;29(1):33–45.
[52] Wood SL. Performance of reinforced concrete buildings during the 1985 Chile earthquake: implications for the design of structural walls. Earthq Spectra 1991;7(4).
[53] Wood SL. Minimum tensile reinforcement requirements in walls. ACI Struct J 1989;86(4):582–91.